EULER EQUATIONS APPLIED TO FLOW OVER NACA0012

Bruno Goffert, bruno_goffert@hotmail.com
Universidade de Taubaté, Rua Daniel Danelli s/n, Jardim Morumbi, Taubaté, 12060-440

João Batista Pessoa Falcão Filho, jb.falcao@ig.com.br
Instituto de Aeronáutica e Espaço, Praça Mal. Eduardo Gomes, 50, São José dos Campos, 12228-904

Abstract. *A fast, accurate numerical code based on implicit resolution of the Euler Equations was used to determine the main flow parameters over a NACA 0012 profile in order to compare them with experimental results obtained in a transonic wind tunnel (PTT – Pilot Transonic Wind Tunnel of IAE, Institute of Aeronautics and Space). To carry out the test campaigns with sounding vehicles of IAE in PTT, many attempts are made to gain expertise, accuracy and to obtain better treatment of wall corrections. Among all the calibration procedures, a NACA 0012 profile is going to be used to compare experimental data with well known results from other tunnels and from theoretical calculation – a bi-dimensional model equipped with pressure taps along the chord will be fixed at the lateral walls to allow angle of attack variation. In this sense, CFD appears as a skilled tool to help obtaining theoretical results. The present work describes the main characteristics of a developed numerical code applied to bi-dimensional geometries, and presents the results obtained with the NACA 0012 for Mach number range from 0.3 to 0.8 at various angles of attack. The code was originally based on the Beam and Warming centered finite-difference, alternating-direction-implicit algorithm, applied to a bi-dimensional, body-conforming system of coordinates, with the time marching using first-order Euler approximation. The code was later modified to follow the diagonal algorithm, firstly developed by Pulliam and Chaussee. Therefore, the final version is fast and robust for non transient problems. This is particularly important for the present research, when many flow cases must be investigated. A special C-type generated mesh was constructed with its external frontier distant about 30 chords from the profile leading edge, and, in order to better treat the near wall region, a node location stretching of 12% was employed. An overall grid refinement and external frontier distance analysis were performed, in order to guarantee an adequate numerical calculation resolution. Results of pressure and Mach number fields are presented and analyzed, and special attention is given to the shape and location of the sonic and shock wave lines, comparing them with the results obtained from literature. Particularly, pressure coefficient over the profile surface is compared with the literature and with tunnel results.*

Keywords*: CFD, Euler Equations, NACA 0012, Pilot Transonic Wind Tunnel*

1. INTRODUCTION

The advance of aeronautical technology is increasing, and every day it is necessary to use the computation as a supporting tool to facilitate the optimization in experimental tests results, reducing cost and time. Due to the increasing interest in numerical simulation in compressible flow over complex surfaces, the CFD technique has improved and nowadays there are many robust and efficient numerical codes to obtain satisfactory aerodynamic results (Yagua *et al.*, 1998). It is of fundamental importance the wind tunnels tests and obtaining reliable experimental results requires a better understanding of the physics involved. There are many factors that may cause distortions of flow over the profile, resulting in values not so equal than in real conditions of flight. Many reasons explain this fact, such as (Rasuo, 2006): Reynolds number effects, Mach number effects, wall tunnel interference, and boundary layers from the side walls. In order to assess the physical phenomena in the PTT (Pilot Transonic Wind Tunnel), a numerical code was developed to help comparing the results.

PTT is now carrying out test campaigns with two sounding vehicles of IAE and this work will be helpful to gain expertise and accuracy, mainly in predicting wall correction parameters during calibration procedures. PTT has a test section width of 0.30 m and a height of 0.25 m. Its circuit is conventional closed, pressurized from 0.5 bar to 1.2 bar, with Mach number range from 0.2 to 1.3. The tunnel is continuously driven by a two-stage 830 kW main compressor, with automatic controls of rotational speed, and stagnation pressure and temperature, in order to guarantee correct adjustment of Mach and Reynolds numbers related to the test section. The tunnel has also an injection system which operates intermittently with the main compressor extending the tunnel operational envelope without penalizing the installed power. More details are available in Falcão Filho and Mello (2002).

The numerical code used was originally based on Beam and Warming centered finite-difference method to solve the Navier Stokes Equations applied for non-viscous flow, called Euler Equations (Beam and Warming, 1978). The Euler Equations have been very used to represent transonic flows because it is able to capture the mixed flow effects (subsonic and supersonic) (Camilo, 2003), conditions frequently found in transonic regimes.

2. MATHEMATICAL MODELING

The Euler Equations written in bi-dimensional generalized body-conforming coordinates, and in conservation-law form is given by (Anderson *et al.*, 1984)

$$\frac{\partial \overline{Q}}{\partial \tau} + \frac{\partial \overline{E}}{\partial \xi} + \frac{\partial \overline{F}}{\partial \eta} = 0 ,$$

(1)

and, the variable-conserved vector is given by

$$\overline{Q} = J^{-1}\begin{bmatrix} \rho & \rho u & \rho v & e \end{bmatrix},$$

(2)

where ρ is density, u and v are velocity cartesians coordinates and e is total energy.
    And the non-viscous flux vectors are

$$\overline{E} = J^{-1}\begin{bmatrix} \rho U \\ \rho u U + p\xi_x \\ \rho v U + p\xi_y \\ (e+p)U - p\xi_t \end{bmatrix},$$

(3)

$$\overline{F} = J^{-1}\begin{bmatrix} \rho V \\ \rho u V + p\eta_x \\ \rho v V + p\eta_y \\ (e+p)V - p\eta_t \end{bmatrix},$$

(4)

where p is static pressure. Adopting the perfect gas hypotheses, p may be expressed by

$$p = \rho(\gamma-1)\left[\frac{e}{\rho} - \frac{1}{2}(u^2 + v^2)\right].$$

(5)

    The curvilinear coordinate system is defined such that ξ is the direction following the airfoil surface, as indicated in Fig. 4, represented by the computational direction i, and η is the radial-like direction from the points on the airfoil surface to the outer frontier, represented by the computational direction j. This coordinate system is obtained from the Cartesian system (x, y) through the relations:

$$\tau = t ,$$

(6)

$$\xi = \xi(t, x, y),$$

(7)

$$\eta = \eta(t, x, y),$$

(8)

and the transformation jacobian is given by

$$J = (x_\xi y_\eta - x_\eta y_\xi)^{-1}.$$

(9)

    The contra-variant velocity components are defined as:

$$U = \xi_t + \xi_x u + \xi_y v ,$$

(10)

$$V = \eta_t + \eta_x u + \eta_y v .$$

(11)

2.1. NUMERICAL IMPLEMENTATION

The code used was originated from the implicit approximate factorization proposed by Beam and Warming (1978), for which the space derivatives are approximated using centered schemes, and the time marching is undertaken through implicit Euler method. To simplify the numerical code and consequently to reduce computational cost, the code was adapted to follow the diagonal algorithm of Pulliam and Chaussee (1981) complemented by a non-linear, spectral-radius-based artificial dissipation strategy due to Pulliam (1986). This implementation maintains the whole stability characteristics and accuracy for stationary state applications (Falcão Filho, 2006). Normally centered schemes are stable only with the use of artificial dissipation and this combination leads to difficulties in capturing flow discontinuities, like shock waves. The use of simple schemes results in passages through shocks not so well defined, as, for example, those oscillations that occur in the pre-shock and post-shock regions (Pulliam, 1986). So, a more sophisticated, non-linear, spectral-radius-based artificial dissipation strategy was implemented to the code (Pulliam, 1986, Mello, 1994, Falcão Filho, 2006). In this way, the shock passage can be well captured like those obtained with upwind schemes.

2.2. STATEMENT OF THE PROBLEM

The simulation was applied to a C-type grid conforming the NACA 0012 for Mach number range from 0.3 to 0.8 at various angles of attack at standard atmospheric conditions. The NACA 4-digit thickness distribution, with x chordwise coordinate, is given by (Menezes, 1994)

$$\frac{y}{c} = \frac{t}{c}\left[a_0\sqrt{\frac{x}{c}} - a_1\left(\frac{x}{c}\right) - a_2\left(\frac{x}{c}\right)^2 + a_3\left(\frac{x}{c}\right)^3 - a_4\left(\frac{x}{c}\right)^4 \right], \tag{12}$$

where $a_0 = 1.4845$, $a_1 = 0.6300$, $a_2 = 1.7580$, $a_3 = 1.4215$, $a_4 = 0.5075$, c is the chord and t maximum thickness (in the present case, $t = 0.12$). This definition results in a small but finite trailing edge thickness. Many computational methods require a zero thickness trailing edge, mainly in order to simplify the calculating mesh. Sometimes the coefficient definitions are modified to produce a zero thickness trailing edge, but this can lead to the wrong values of aerodynamic proprieties. The geometry adopted herein was the original one and an additional grid point just after the trailing edge represents the zero thickness. Figure 1 shows the trailing edge constructed, where the dashed line represents the end of the airfoil according to Eq. 12. The total length was increased about 0.9%.
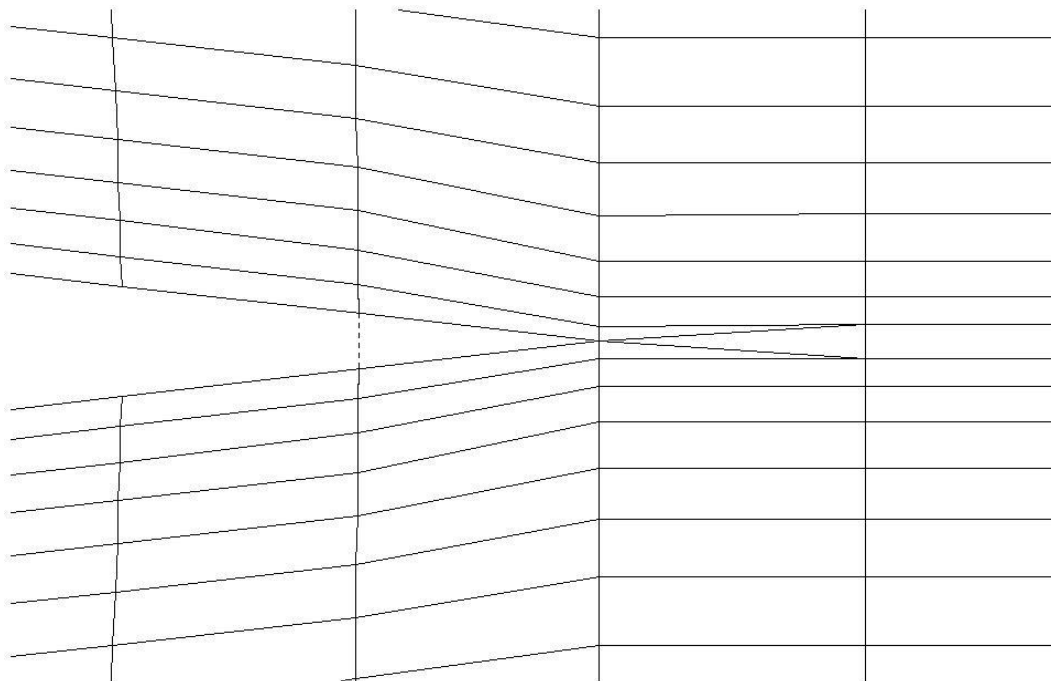

Figure 1. Trailing edge modification detail.

A first mesh with 329 x 70 points was constructed to represent the whole field with the external frontiers distant about 30 chords from trailing edge, as shown in Fig. 2.
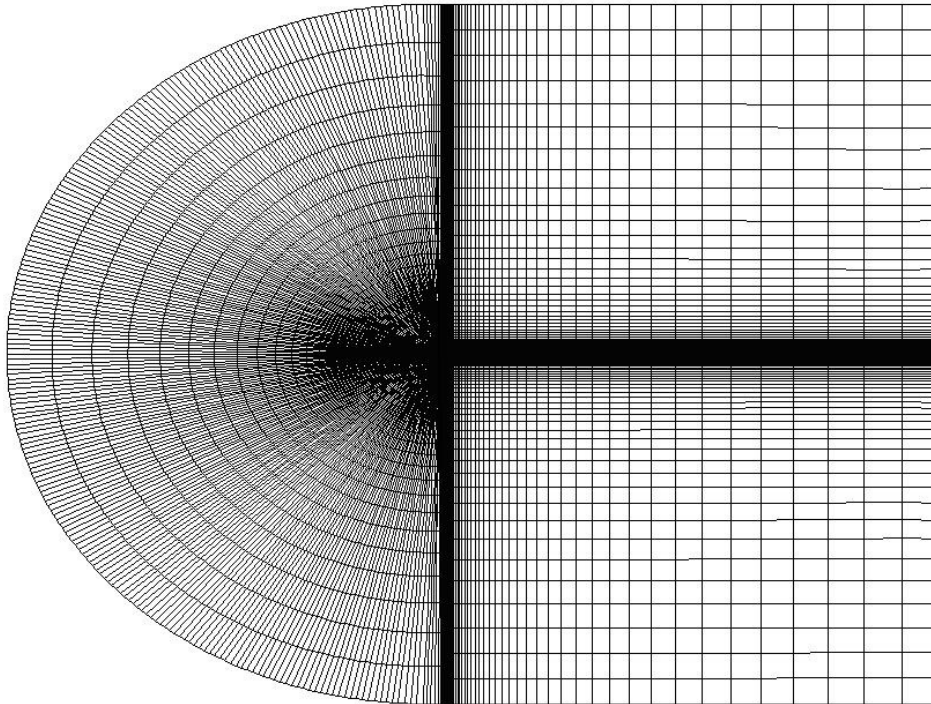
Figure 2. Structured type C grid about NACA 0012 airfoil.

A stretching of 12% was used to better represent regions near solid frontier, as it is shown in Fig 3. After the trailing edge a dispersion of points was made to decrease the field clustering, facilitating the computational process.
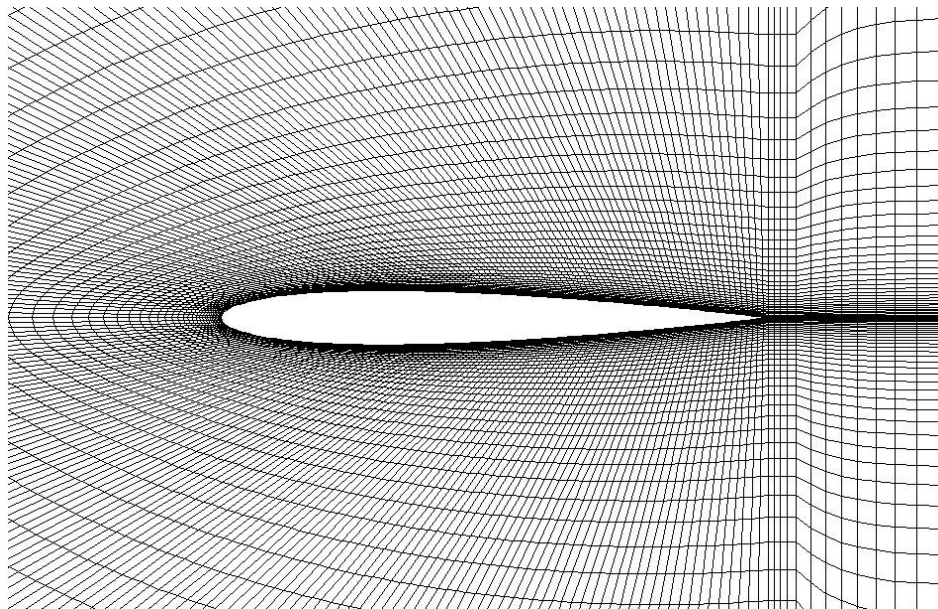

Figure 3. Grid near NACA 0012 airfoil.

A grid refinement effect was investigated using two more meshes, a coarser one, with 165 x 35 points, and a finer one, with 657 x 139 points. These new meshes were obtained from the original one, manipulating the even order points, being kept the same physical geometry.

2.2.1. BOUNDARY CONDITIONS

The boundary conditions were treated differently in three distinct regions: external frontiers, airfoil surface and the mesh frontier in the wake region, as pointed in Fig. 4.
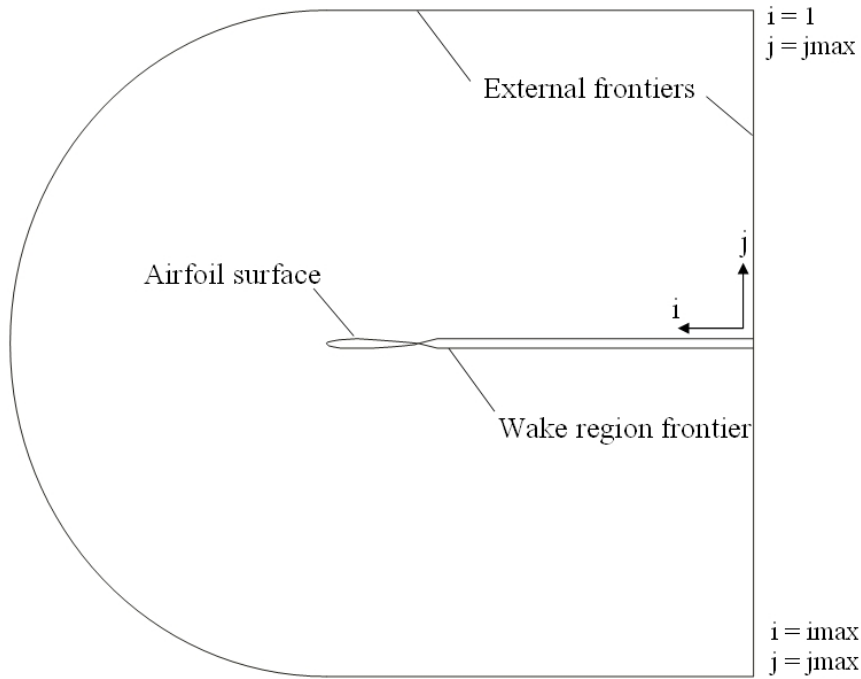
Figure 4. Mesh scheme showing the boundaries.

The outer frontier was treated in a very simple way. Admitting that it is far enough from the airfoil surface and the pressure disturbances do not affect the pressure distribution over the airfoil surface, it was used zeroth-order extrapolation to the flow parameters (Hoffman and Chiang, 2000): temperature, T, density, ρ, and velocity components u and v.

For $i = 1$,

$$T_{i,j} = T_{i+1,j}, \; \rho_{i,j} = \rho_{i+1,j}, \; u_{i,j} = u_{i+1,j}, \; v_{i,j} = v_{i+1,j}. \tag{13}$$

For $i = imax$,

$$T_{i,j} = T_{i-1,j}, \; \rho_{i,j} = \rho_{i-1,j}, \; u_{i,j} = u_{i-1,j}, \; v_{i,j} = v_{i-1,j}. \tag{14}$$

And for $j = jmax$,

$$T_{i,j} = T_{i,j\max-1}, \; \rho_{i,j} = \rho_{i,j\max-1}, \; u_{i,j} = u_{i,j\max-1}, \; v_{i,j} = v_{i,j\max-1}. \tag{15}$$

Over the profile the temperature was extrapolated from the first calculating internal point, considering adiabatic wall. The same was done to pressure, resulting

$$T_{i,j} = T_{i,j+1}, \; p_{i,j} = p_{i,j+1}. \tag{16}$$

According to the Euler Equations flow physics applied to a solid frontier, a slip wall condition must be established. It is specified by setting the normal component of velocity equal to zero, while allowing tangential component of the velocity. In this way the flow is forced to be always tangent to the solid frontier (Blazek, 2001, Hoffmann and Chiang, 2000). Thus, for curvilinear coordinates, at $j = 1$,

$$U_{i,j} = U_{i,j+1}, \tag{17}$$

$$V_{wall} = 0. \tag{18}$$

By manipulating Eqs. (10), (11), (17) and (18), one can find

$$v_{(i,j)} = -\frac{\eta_{x(i,j)} u_{(i,j)}}{\eta_{y(i,j)}}, \tag{19}$$

$$u_{(i,j)} = \frac{\xi_{x(i,j+1)} u_{(i,j+1)} + \xi_{y(i,j+1)} v_{(i,j+1)}}{\xi_{x(i,j)} - \dfrac{\xi_{y(i,j)} \eta_{x(i,j)}}{\eta_{y(i,j)}}}. \tag{20}$$

The mesh branches upper and lower to the airfoil wake region were conceived to be mutually overlapped as shown in Fig. 5. The points over the boundary line that goes to the left (see the arrow), ($j = 1$ in the upper region of the mesh), marked with "+" in the figure, coincide with the points over the first line of the calculus domain that goes to the right ($j = 2$), marked with squares. And the points over the boundary line that goes to the right ($j = 1$ in the lower region of the mesh), marked with "x", coincide with the points over the first line of the calculus domain that goes to the left ($j = 2$), marked with circles. This way, it is not necessary establish any condition at the boundaries of the mesh, because the parameters have the same values of the inner region of the overlapped mesh. So, all the points in the wake region are calculated. The values of parameters are just transferred from the inner region to the boundary line.
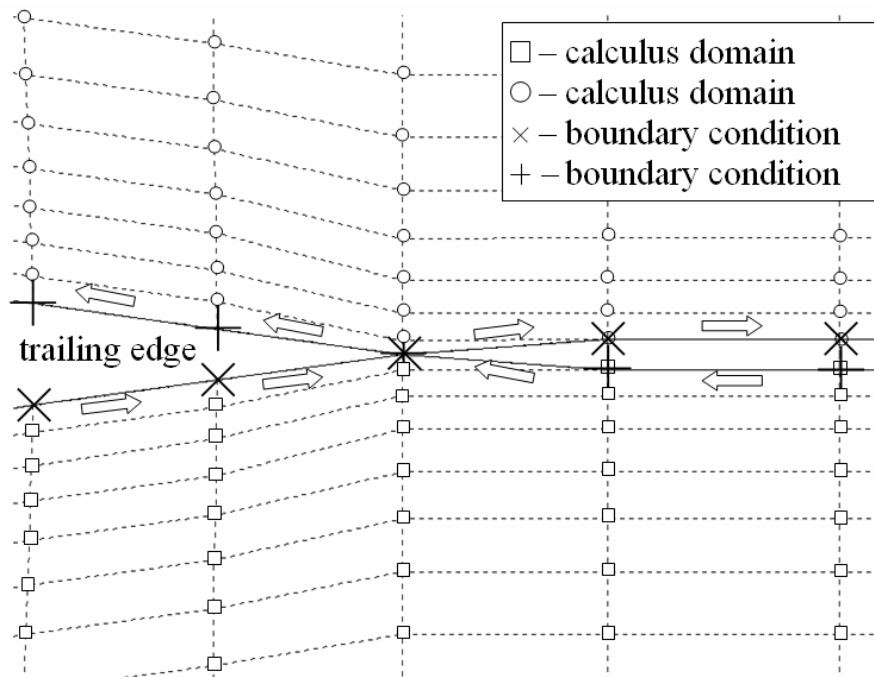

Figure 5. Boundary conditions scheme in the wake region.

There are some other possible approaches to this issue. Normally the mesh is created in such a way that the boundary points (at $j = 1$) from the upper side of the mesh precisely coincide with the boundary points from the lower side. So, these points cannot be calculated. They must be established by boundary conditions. A more precise way to treat this region is to develop specific equations (from the Euler approach) for the common line, using neighbor points from the inner region (calculus domain) – this approach has some difficulties to be implemented. Another very simple way found in literature is to attribute averaged values taken from the upper and lower neighbors (Menezes, 1994), provided that the local grid refinement is adequate. However, the approach used herein is easier to implement, and of course, it represents the real physics, once the chosen mesh guarantees that.

3. RESULTS

For all cases simulated the mesh used had 329 x 70 points, and the external frontiers were distant 30 chords from the leading edge. Among them, the three most significant cases will be addressed herein.

The first case was carried out with flow conditions at Mach number equal to 0.3 and angle of attack of 1.86°. This numerical calculation had fast convergence and Figs. 6 and 7 show pressure and Mach number fields over the profile.

The pressure field showed good behavior with the expected physics, reaching a maximum value near the leading edge of 6.6% of far field pressure. The maximum Mach number observed was 0.4 in the upper camber region. Figure 8 shows how well the comparisons with other code and the experimental data were.
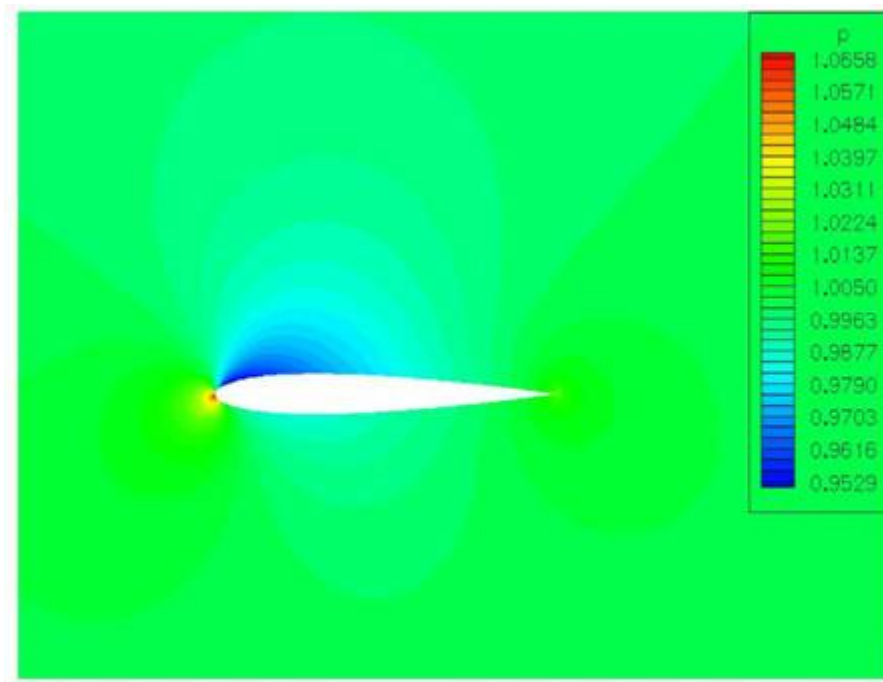

Figure 6. Pressure coefficient contour for $M_\infty = 0.3$ and angle of attack of 1.86°.

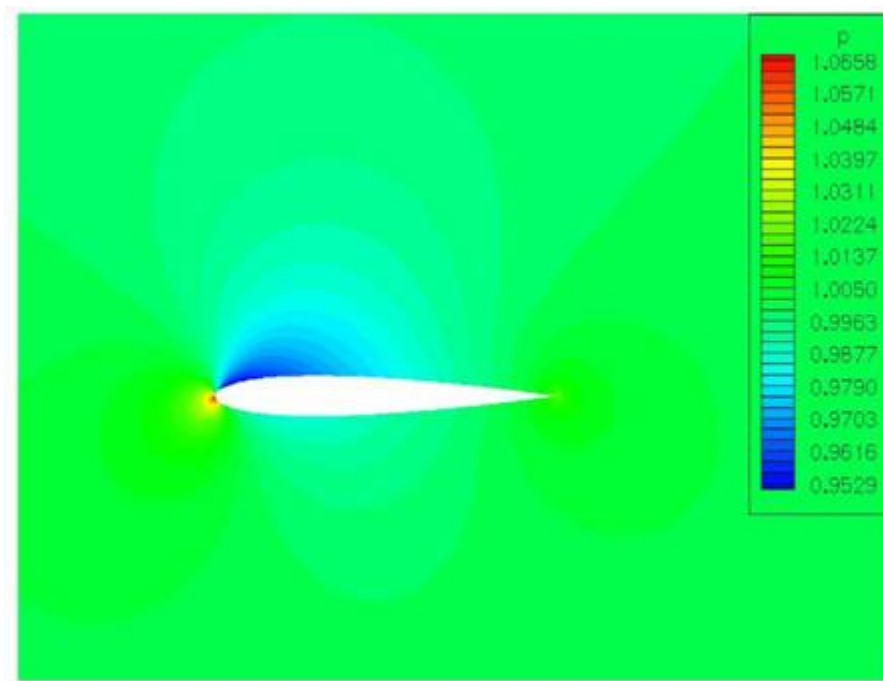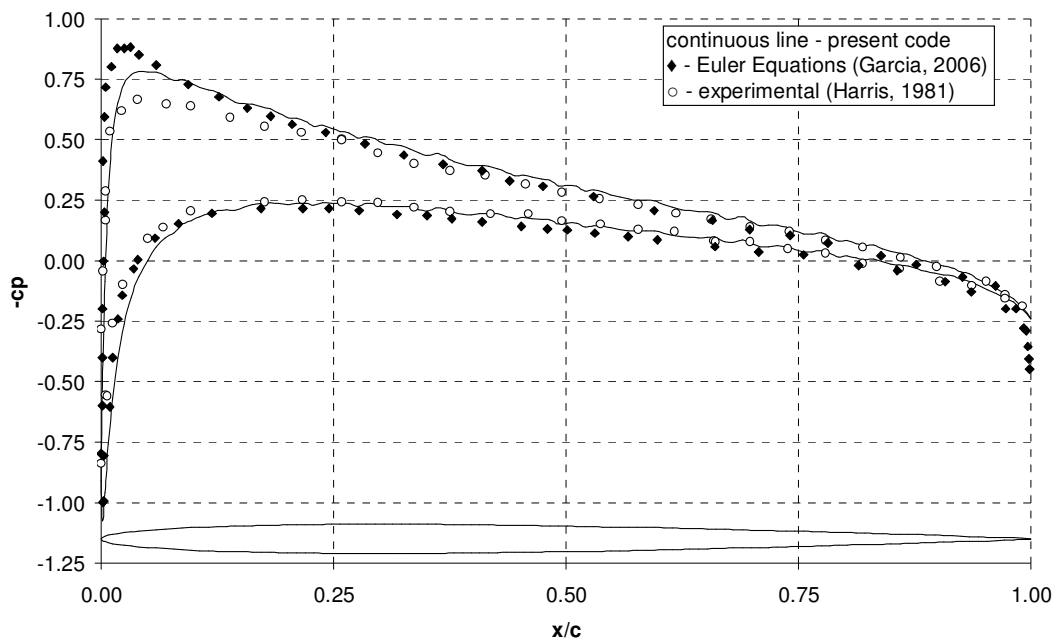Figure 7. Mach number contour for $M_\infty = 0.3$ and angle of attack of 1.86°.

Figure 8. Pressure coefficient distribution along the chord for $M_\infty = 0.3$ and angle of attack of 1.86º.

A second study case with Mach number 0.63 and angle of attack of 2º was carried out. Figure 9 shows the resulted Mach number field. This case is particularly significant because it corresponds to a critical Mach number condition. In the figure it is possible to observe a sonic point at somewhere on the airfoil upper surface.
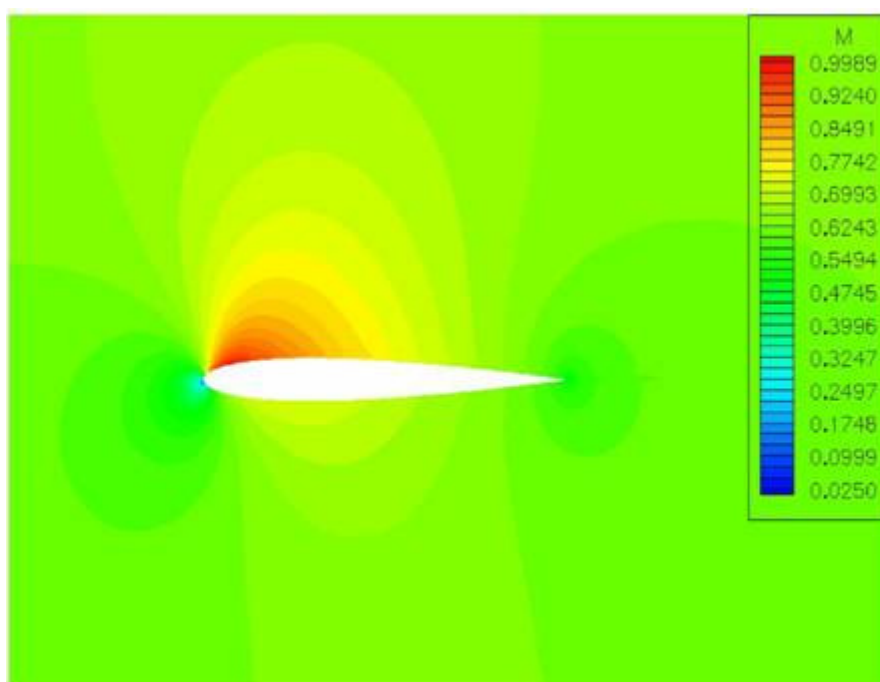

Figure 9. Mach number field for $M_\infty = 0.63$ and angle of attack of 2.00º.

Finally, a third case with Mach number 0.8 and angle of attack zero was investigated – see Figs. 10 and 11. The overpressure in the leading edge reached about 50% of free-stream value. This case presented a strong shock wave located approximately at 50% of chord. In fact, the transonic regime complicated the convergence, causing the pressure contours near the wall to be not so well defined – the reason for that is the numerical oscillations due to the local refinement. In both figures it is possible to observe how well is the shock wave line defined. This fact demonstrates the superior characteristic of the special artificial dissipation used in capturing the shock waves passages. A better prove is

shown in Fig. 12 where pressure coefficient distribution calculated along the chord is compared with other results from the literature.

The present code followed the general tendency of other works, however the shock wave position occurred a little later. The pressure coefficient drop through the shock wave was more abrupt also, being recovered to the common level afterwards. Probably the perturbation after the shock happened due to numerical oscillations. The shock wave resembles a normal shock. The Mach number through it changed from 1.30 to 0.82, and the pressure increased 74.4%, value lower than the corresponding value founded in normal shock, 80.5% (Zucker, 1977).
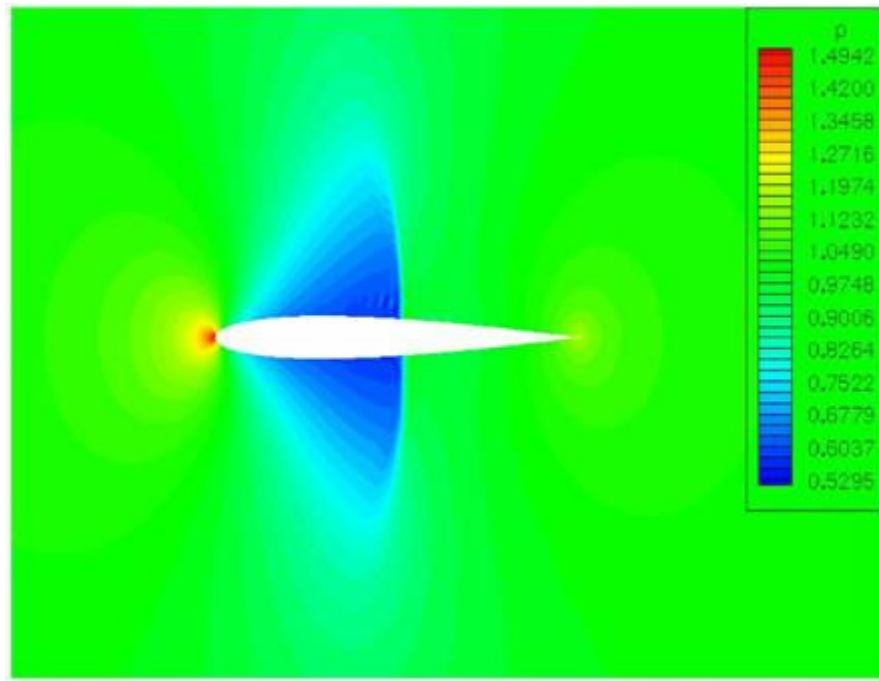
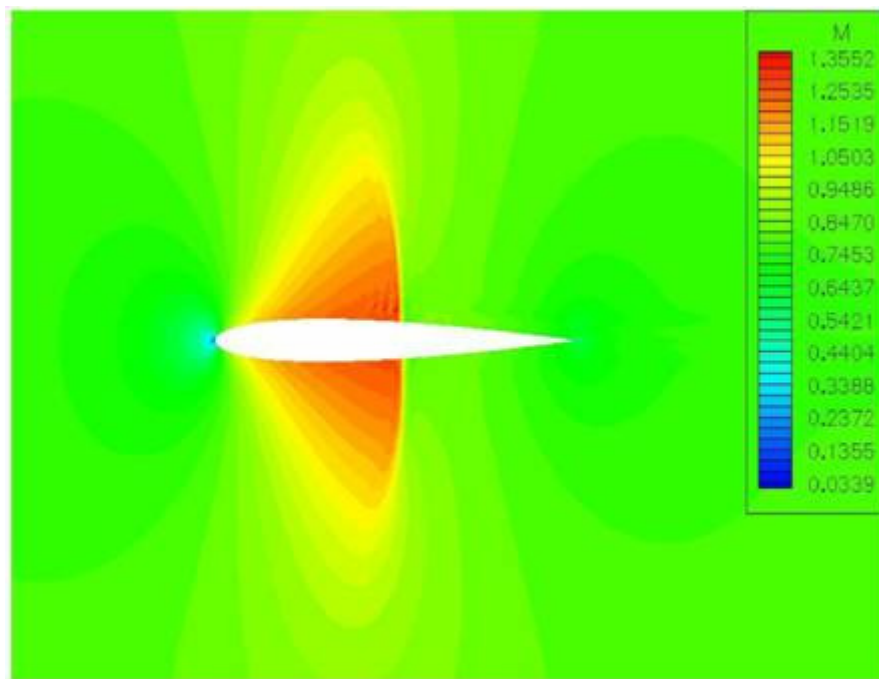Figure 10. Pressure field for $M_\infty = 0.8$ and angle of attack of 0º.

Figure 11. Mach number field for $M_\infty = 0.8$ and angle of attack of 0º.
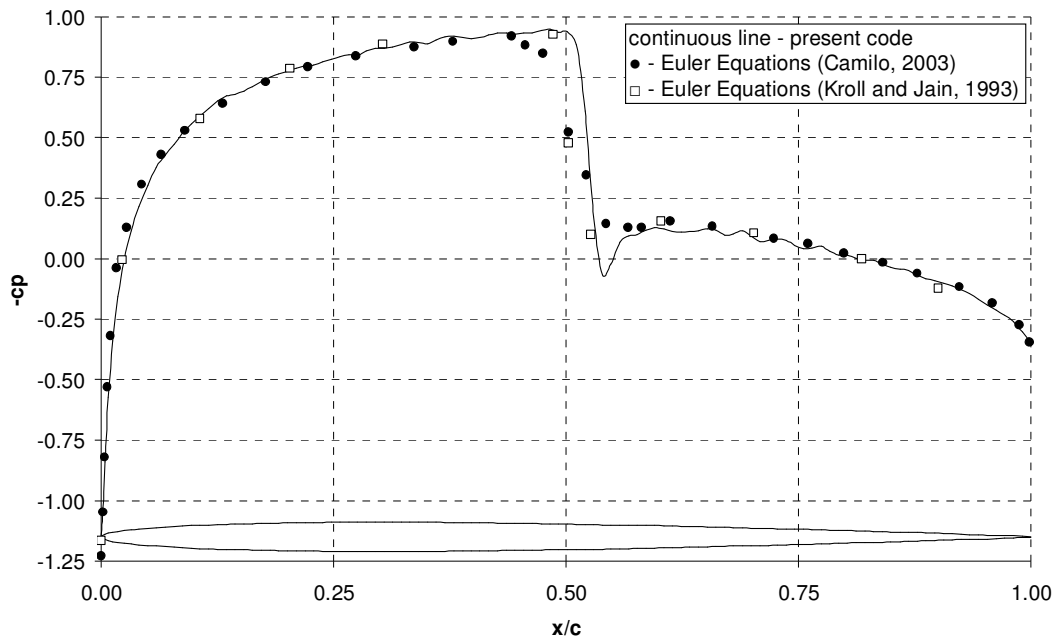
Figure 12. Pressure coefficient distribution along the chord, for $M_\infty = 0.8$ and angle of attack of 0°.

To evaluate the mesh refinement, three different grids with 657 x 139, 329 x 70 and 165 x 35 points were used. The Mach number was 0.5 and the angle of attack was 5.86°. Figure 13 shows the pressure coefficient distribution along the airfoil chord. It can be observed the convergence tendency as the mesh is more refined. Although discrepancies can still be noticed, the results prove that the intermediary mesh has already good agreement with the finer one. Besides that, the use of the finest mesh (657 x 139) took many hours to convergence, being considered not adequate for the present research.
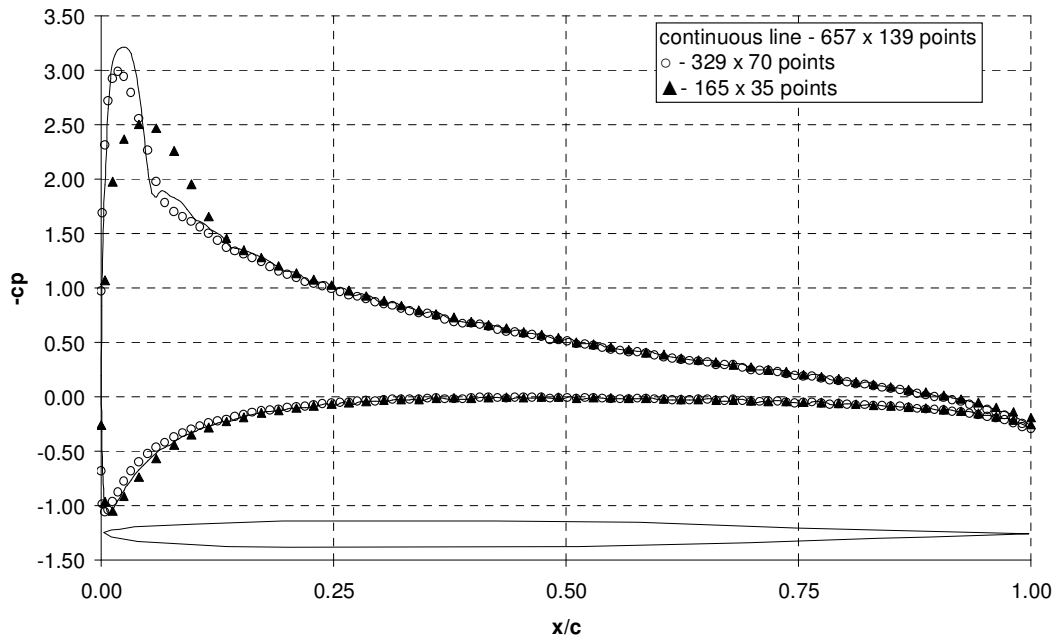

Figure 13. Comparisons of pressure coefficient distribution, using three different mesh refinements, for $M_\infty = 0.5$ and angle of attack of 5.86°.

Normally it is expected that disturbances which reaches the outer frontier may return to the calculation field. This problem can be better treated if, for example, the Riemann´s invariant is used at the outer boundary (Blazek, 2001).

Herein a simple extrapolation was chosen (see item 2.2.1), and this causes disturbances and, consequently, errors in the final result. So, it is necessary to verify the effects of these disturbances when the outer frontier is much more distanced from the airfoil. To check this, a special mesh 10 times bigger was created (with radius of 300 chords). The flow parameters were: Mach number of 0.7 and angle of attack of 1.86°. The result is shown in Fig. 14, and prove that it is not necessary a bigger than 30 chords mesh. The shock wave was well captured in both meshes with very small discrepancy of pressure coefficient along the chord.
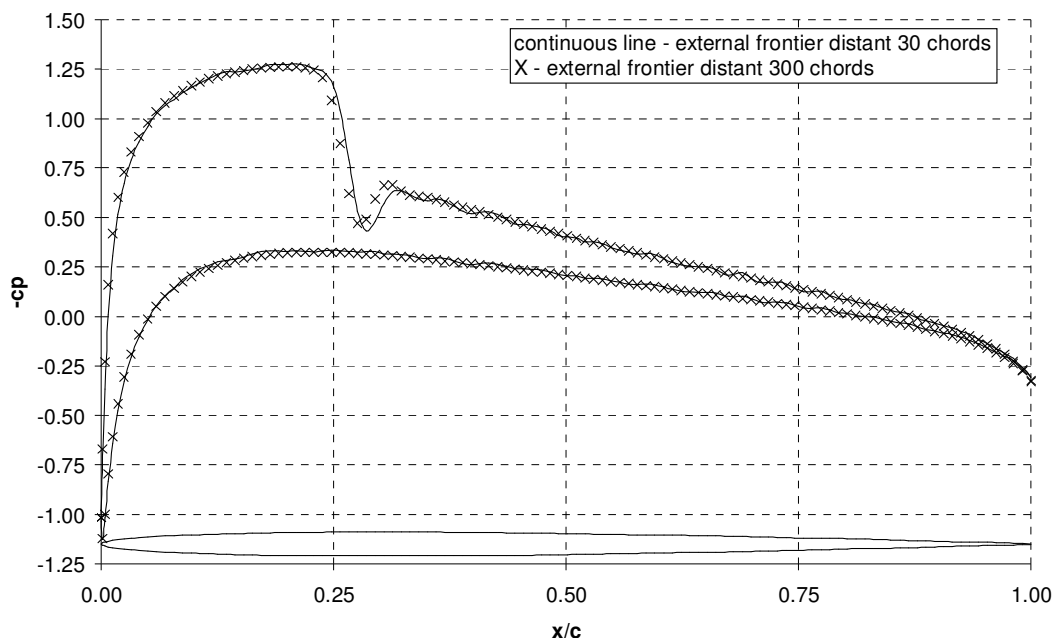

Figure 14. Comparison of pressure coefficient distribution varying the distance of external frontiers for $M_\infty = 0.7$ and angle of attack of 1.86°.

4. CONCLUSIONS

A CFD code is presented, based on the Beam and Warming implicit method and modified to follow the diagonal algorithm of Pulliam and Chaussee for Euler Equations. It is described the boundary conditions treatment for a structured C-type mesh, especially constructed for running three study cases. It was described a special strategy, by overlapping the mesh over itself, facilitating enormously the boundary conditions treatment in the wake region.

A grid effect investigation was carried out, using three differently refined meshes. And also the mesh size was verified with a mesh 10 times wider to analyze the outer frontier distance effect. In both cases, the choices used herein proved to have good characteristics.

For the cases of study, the physical phenomena were assessed by observing the main flow parameters (pressure and Mach number) in the whole calculated field.

The pressure coefficient distribution over the NACA 0012 airfoil was compared with the results from other codes and experimental tests, and it was proved to be satisfactory. The good quality of the results will be very useful in the future to compare with the experimental results obtained at PTT.

5. ACKNOWLEDGEMENTS

6. REFERENCES

Anderson, D. A., Tannehill, J. C., Pletcher, R. H., 1984, *Computational Fluid Mechanics and Heat Transfer*, Hemisphere Publishing Corp.
Beam, R. M., Warming, R. F., 1978, "An Implicit Factored Scheme for the Compressible Navier Stokes Equations", *AIAA Journal*, Vol. 16, n°4.

Blazek, J., 2001, *Computational Fluid Dynamics: Priciples and Applications*, Elsevier Science Ltd., Oxford, pp. 267-284.

Camilo, E., 2003, "Solução Numérica das Equações de Euler para Representação do Escoamento Transônico em Aerofólios", Tese de Mestrado, Universidade de São Paulo, São Carlos, pp. 1-65.

Falcão Filho, J. B. P., Mello, O. A. F., 2002, "Descrição Técnica do Túnel Transônico Piloto do Centro Técnico Aeroespacial," Proceedings of the 9th Brazilian Congress of Thermal Engineering and Sciences, Caxambu-MG.

Falcão Filho, J. B. P., 2006, "Estudo Numérico do Processo de Injeção em um Túnel de Vento Transônico", Dissertação de Doutorado, Instituto Tecnológico de Aeronáutica, São José dos Campos.

Garcia, O. M. A., 2006, "Numerical Simulations of Compressible Flows over Airfoils", Tese de Mestrado, Instituto Tecnológico de Aeronáutica, São José dos Campos.

Harris, C. D., 1981, "Two Dimensional Aerodynamic Characteristics of the NACA 0012 Airfoil in the Langley 8 Foot Transonic Pressure Tunnel", NASA-TM-81927.

Hoffman, K. A., Chiang, S. T., 2000, *Computational Fluid Dynamics*, Engineering Education System, Wichita, Kansas.

Kroll, N., Jain, R. K., 1987, "Solutions of the Two-Dimensional Euler Equation – Experience with Finite Volume Code", DFVLR-FB 87-41, apud Oliveira (1993).

Mello, O. A. F., 1994, "An Improved Hybrid Navier-Stokes: Full-Potential Method for Computation of Unsteady Compressible Viscous Flows", PhD Dissertation, Georgia Institute of Technology, Atlanta.

Menezes, J. C. L., 1994, "Análise Numérica de Escoamentos Transônicos Turbulentos em Torno de Aerofólios", Tese de Mestrado, Instituto Tecnológico de Aeronáutica, São José dos Campos.

Pulliam, T. H., 1986, "Artificial Dissipation Models for the Euler Equations", *AIAA Journal*, Vol. 24, nº12.

Pulliam, T. H., Chaussee, D. S., 1981, "A Diagonal Form of an Implicit Aproximate-Factorization Algorithm", *Journal of Computational Physics*, Vol. 39.

Rasuo, B., 2006, "An Experimental and Theoretical Study of Transonic Flow about NACA 0012 Airfoil", AIAA 2006-3877, 24th Applied Aerodynamics Conference, San Francisco.

Yagua, L. C. Q., Basso, E., Azevedo, J. L. F., 1998, "Bidimensionais em Escoamentos Compressíveis," Proceedings of the 7th Brazilian Congress of Thermal Engineering and Sciences, Rio de Janeiro.

Zucker, R. D., 1977, *Fundamentals of Gas Dynamics*, Matrix Publishers Inc., Beaverton, Oregon.

7. RESPONSIBILITY NOTICE

The authors are the only responsible for the printed material included in this paper.